Environmental Science and Pollution Research (2021) 28:28507–28517
https://doi.org/10.1007/s11356-021-12598-2

RESEARCH ARTICLE

Insight into the effect of pH-adjusted acid on thermodynamic properties and crystallization sequence during evaporative-crystallization process of hydrolyzed urine

Shanqing Jiang[1,2] · Xiang Xing[1] · Liping Wang[1] · Shengjiong Yang[2] · Jingwen Xiao[1] · Qiuya Zhang[1,2] · Xia Xu[1] · Mingguo Peng[1] · Xiaochang Wang[2]

Received: 16 September 2020 / Accepted: 18 January 2021 / Published online: 4 February 2021
© The Author(s), under exclusive licence to Springer-Verlag GmbH, DE part of Springer Nature 2021

Abstract

The evaporative-crystallization process (ECP) is a frequently used approach for complete nutrient recovery from human urine, and crystallization sequence is related to the selection of seed and the optimization of crystallization process. In this study, three hydrolyzed urine (HU) samples, which were acidified to an initial pH of 4 with HCl, H_2SO_4, and H_3PO_4, were used to recover crystallized products by ECP, their crystallization process and thermodynamic properties during ECP were compared, and the detailed crystallization sequence was analyzed using the PHREEQC-2 simulation. The results showed that the pH-adjusted acid has a significant effect on crystal precipitation, and the new crystal in HCl-4-HU, H_2SO_4-4-HU, and H_3PO_4-4-HU first appeared at volume concentration factors (CF_V) of 19.61, 9.90, and 9.96, respectively. Furthermore, the simulated crystallization process characteristics of HU by PHREEQC-2 have a good fit with the actual experimental data, and crystallization sequence of HCl-4-HU, H_2SO_4-4-HU, H_3PO_4-4-HU during ECP were NH_4Cl (CF_V from 10.25 to 100) / NaCl (CF_V from 71.43 to 100), NH_4NaSO_4 (CF_V from 10.25 to 55.56) / NH_4Cl (CF_V from 20 to 100) / $(NH_4)_2SO_4$ (CF_V from 40.45 to 100), $NH_4H_2PO_4$ (CF_V from 10.25 to 100) / NaH_2PO_4 (CF_V from38.46 to 55.5) / NaCl (CF_V from 45.46 to 100), respectively. The present study clearly reveals the crystallization sequence and thermodynamic properties of nutrient elements in acidified HU, which provides an important theoretical basis for the optimization of crystallized products obtained from HU for future study.

Keywords Human urine · pH-adjusted acid · Volume concentration factor · Crystallization sequence · Pitzer Model

Abbreviations

ECP	Evaporative-crystallization process
HU	Hydrolyzed urine
CF_V	Volume concentration factors
$V_{con.}$	Volume of concentrated HU
CF_D	Detected concentration factor
CF_N	Normalized concentration factor
IAP	Ion activity product
Ks	Solubility product
TAN	Concentrations of total ammonia

Responsible Editor: Philippe Garrigues

✉ Shanqing Jiang
jiangshanqing@cczu.edu.cn

✉ Xiaochang Wang
xcwang@xauat.edu.cn

[1] School of Environmental and Safety Engineering, Changzhou University, Changzhou 213164, China

[2] School of Environmental and Municipal Engineering, Xi'an University of Architecture and Technology, Xi'an 710055, China

Introduction

Human urine is part of the domestic sewage, which contains the main nutrient with approximately 80% nitrogen (N), 50% phosphorus (P), and 70% potassium (K) (Chipako and Randall 2020; Volpin et al. 2019). Moreover, the content of N, P, and K in urine is balance, and their proportion is consistent with the nutrient demands of general crops, which can be directly utilized as a liquid fertilizer after 6 months of storage and was widely used in some rural and suburban areas, such as Tai Lake Region in China (Karak and Bhattacharyya 2011; Pronk and Koné 2009). Thus, the urine separation and nutrient recovery are consistent with sustainable development; they can reduce almost 20% of agricultural fertilizer requirements

and over 80% of the total load of N and P in sewage plants (Alemayehu et al. 2020; Malila et al. 2019). However, the large storage capacities and high transportation cost limit the direct use of liquid urine as fertilizer on a large scale (Alemayehu et al. 2020). Therefore, technologies for on-site nutrient recovery as solid products from urine are favorable and urgently required.

Till now, various techniques are used for the in situ recovery of nutrients from urine, such as ammonia stripping (Jiang et al. 2016; Tao et al. 2019), struvite crystallization (Barbosa et al. 2016; Huang et al. 2019a; Huang et al. 2019b), and adsorption (Jiang et al. 2016; Liu et al. 2020; Xu et al. 2018). Ammonia stripping can recover only N in urine (Tao et al. 2019); struvite crystallization can recover N, P, and K as precipitates of $MgNH_4PO_4{\cdot}6H_2O$ and/or $MgKPO_4{\cdot}6H_2O$, but the recovery rate of N and K is less than 10% without a P source (Barbosa et al. 2016; Huang et al. 2019a; Huang et al. 2019b). Different ionic charges between NH_4^+/K^+ and PO_4^{3-} make it difficult for adsorption materials to simultaneously adsorb N, P, and K (Liu et al. 2020; Xu et al. 2018). Combination of two or three techniques, such as ammonia stripping followed by a struvite-K precipitation or ammonia stripping combined with an adsorption of P and K, can recover N, P, and K together, but the combination processes will bring complex operation problems. On the other hand, dehydration techniques such as evaporation (Antonini et al. 2012; Jiang et al. 2017), freeze-thaw (Gulyas et al. 2004; Randall and Nathoo 2018), alkaline dehydration (Simha et al. 2020), and membrane technology (Volpin et al. 2020; Wang and Wei 2020) also can obtain solid products that contain nearly full N, P, and K in urine by concentrating the dissolved salts to their solubility limitation. Among them, evaporation is considered be the most suitable for large-scale application in practice due to its easy operation. Additionally, solar thermal equipment can be applied for urine evaporation in the regions with sufficient sunlight, which can reduce energy consumption, and ultraviolet radiation in sunlight plays a positive role in the degradation of micropollutants and pathogens in urine (Antonini et al. 2012; Jiang et al. 2017).

Human urine usually exists in the form of hydrolyzed urine (HU) with a pH of approximately 9.2 because there are urease-active bacteria in the actual collection and storage system. Thus, minimizing ammonia volatilization is the key to the evaporation process of urine hydrolyzation (Ledezma et al. 2015). Presently, nitrification is used to oxidize 50% NH_4^+ in urine to NO_3^- to stabilize NH_4^+ (Udert and Wächter 2012). However, many ammonia-oxidizing bacteria and nitrite-oxidizing bacteria are required, and strong anti-shock loading capability of system was required, which result in the strict operation and difficult implementation. Compared with nitrification, adding acids such as HCl, H_2SO_4, and H_3PO_4 to hydrolyze urine is the most direct and convenient method to inhibit ammonia volatilization. The optimal initial pH of 4 was determined by considering both N retention and acid consumption in our previous study (Jiang et al. 2017). Furthermore, the final crystallization products of HU acidified by different pH-adjusted acids were significantly different due to the changes in ion composition, which also affects the crystallization process of HU (Jiang et al. 2017). As we know, the addition of a seed to the concentrated urine with the same composition as the crystalline intermediate is beneficial to the crystallization process. Thus, it is necessary to clarify the detailed crystallization sequence during the evaporative-crystallization process, which is related to the thermodynamic properties of the electrolyte (Abdel Wahed et al. 2015). However, till now, few studies clearly revealed this question.

Therefore, the primary objective of this study is to determine the crystallization sequence during the evaporation-crystallization process (ECP) of hydrolyzed urine acidized by three different pH-adjusted acids (HCl, H_2SO_4, and H_3PO_4). More specifically, the main ion concentrations of three acidized hydrolyzed urine at different volume concentration factors were experimentally studied. The thermodynamic characteristics of the crystallization process were analyzed. PHREEEQC-2 was used to simulate the changes in ion concentration in the urine evaporation-crystallization process and analyze the theoretical crystallization sequence. This study provides an important theoretical basis for the optimization of HU crystalline products.

Materials and methods

Collection and pretreatment of urine

Undiluted fresh urine was collected from a modified ordinary urinal (no water flush) in a public male toilet on campus of Xi'an University of Architecture and Technology in China. The urine was completely hydrolyzed after 5~7 days of storage, and it was defined as HU. HU was divided into three portions, and its pH was adjusted to 4 by HCl, H_2SO_4, and H_3PO_4 to make the samples of HCl-4-HU, H_2SO_4-4-HU, and H_3PO_4-4-HU. Their specific physico-chemical properties are shown in Table 1.

Evaporation-crystallization experiments

The installation drawing of evaporation-crystallization experiments is shown in Fig. 1. To reduce the effect of subsequent sampling processes on the accuracy of the experimental data, multiple sets of 1-L flask evaporators were set up and numbered; 500 mL HCl-4-HU, H_2SO_4-4-HU, and H_3PO_4-4-HU were added into the flask evaporators, and their temperature was controlled at 65 °C by heating the bottom of the flask, the generated vapor was condensed by tap water in the cooling coil, and the condensate was collected in a 250-mL beaker containing 50 mL 2% H_3BO_3.

Table 1 The main physical and chemical characteristics of HCl-4-HU, H_2SO_4-4-HU, and H_3PO_4-4-HU in the experiment

	HCl-4-HU		H_2SO_4-4-HU		H_3PO_4-4-HU	
	Mean	±SD	Mean	±SD	Mean	±SD
NH_4^+ (mg/L)	5512.94	257.61	5569.19	431.95	5541.06	508.38
Na^+ (mg/L)	3180.74	137.14	3213.20	262.67	3196.97	332.03
K^+ (mg/L)	1212.59	152.62	1224.96	98.04	1218.77	51.49
Cl^- (mg/L)	15229.14	625.45	5178.43	239.94	5152.27	322.80
SO_4^{2-} (mg/L)	1397.99	82.67	6202.06	477.16	1405.13	131.37
PO_4^{3-} (mg/L)	272.64	34.24	275.42	22.44	8494.05	640.07
pH	4.01	0.11	4.02	0.08	4.01	0.07
EC (mS/m)	56.12	4.23	60.40	4.97	74.28	5.62

Sampling: pH, EC, and volume of concentrated HU ($V_{con.}$) were detected accurately while residue volume of concentrated in flask evaporators was approximately 400, 350, 300, 250, 200, 150, 100, 50, 25, 15, 10 ml, respectively, and concentrated HU was sampling for analysis of NH_4^+, Na^+, K^+, Cl^-, SO_4^{2-}, and PO_4^{3-} concentration, and flask evaporators were not put back. The specific $V_{con.}$ and corresponding volume concentration factor (CF_V) are listed in Table 2. Additionally, for better comparing the concentration difference of different inorganic ions, a normalized concentration factor (CF_N) were defined, which was the ratio of detected concentration factor (CF_D) and CF_V of an inorganic ion during the evaporative-concentration process (Eq. 1),

$$CF_N = \frac{CF_D}{CF_V} \tag{1}$$

where the specific calculation formula of CF_D and CF_V were shown as following (Eq. 2 and 3),

$$CF_D = \frac{C_t}{C_0} \tag{2}$$

$$CF_V = \frac{V_0}{V_{con.}} \tag{3}$$

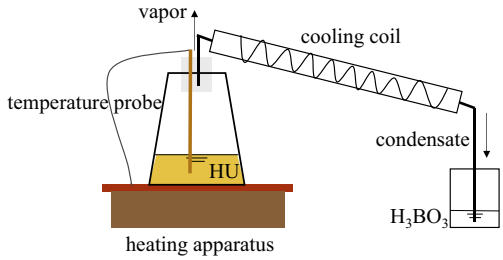

Fig. 1 The experimental installation drawing of evaporation-crystallization of HU

Table 2 The specific volume of concentrated ($V_{con.}$) and corresponding volume concentration factor (CF_V) of HU during the evaporation-concentration process

No.	HCl-4-HU		H_2SO_4-4-HU	H_3PO_4-4-HU		
	$V_{con.}$ (mL)	CF_v	$V_{con.}$ (mL)	CF_v	$V_{con.}$ (mL)	CF_v
1	400.5	1.25	401.0	1.24	399.0	1.25
2	351.5	1.42	350.5	1.42	351.0	1.42
3	301.0	1.66	299.0	1.67	302.0	1.65
4	249.5	2.00	249.0	2.01	250.5	1.99
5	202.5	2.47	200.5	2.49	201.0	2.48
6	151.0	3.31	150.5	3.32	150.0	3.33
7	100.5	4.97	99.0	5.05	102.5	4.87
8	50.6	9.88	50.5	9.90	50.2	9.96
9	25.5	19.61	25.2	19.84	24.8	20.16
10	15.5	32.26	15.0	33.33	15.2	32.89
11	10.4	48.07	10.2	49.02	10.5	47.62

where C_t was the concentration of some ion at the time of t, mg/L; C_t was the initial concentration of some ion, mg/L; $V_{con.}$ was the volume of concentrated HU during ECP, mL; V_0 was the original HU volume before evaporation, mL.

Analysis of crystallization thermodynamic properties

The crystallization equilibrium thermodynamic properties were mainly studied by calculating the solution ion activity coefficient (γ) and ion activity product (IAP). When the IAP of the considered electrolyte in solution reaches or exceeds the solubility product (Ks) of the electrolyte, it means that the salt crystallizes or precipitates (Hajbi et al. 2011; Li et al. 2019b). Presently, the computing methods of γ and IAP are mainly included in the *Specific Ion Interaction Theory Model* (SIT) and *Pitzer Model*. *Pitzer Model* is far more complex than SIT, but Pitzer offers a more accurate model of ionic activity coefficients for hypersaline brines such as urine (Lassin et al. 2018; Yang et al. 2020). Thus, the *Pitzer Model* equation was selected for this study. The detailed computing method by *Pitzer Model* was referred to the research of Ferid et al. in this study (Hajbi et al. 2011).

Chemical simulation of ECP

The simulated evaporation-crystallization process of natural waters (lake water, seawater, etc.) by PHREEQC is widely used because it can remove moles of water from the solution, and PHREEQC is a publicly available, expandable, and well-documented geochemical modeling code with an extensive thermodynamic database (Zhang et al. 2019). HU is essentially a type of water solution containing a high concentration of

inorganic salt, which is similar to the composition of seawater. Hence, PHREEQC was selected to simulate the evaporation-crystallization process of HU, and the crystallization sequence of nutrients in different acid-adjusted HU samples was theoretically analyzed.

Based on PHREEQC-2 modeling of HU evaporation-crystallization process, the following assumptions were made in this study: (1) influence of HU crystallization thermodynamic was considered only and evaporation-crystallization kinetic of the process was ignored, and (2) influence of organics in HU on the evaporation-crystallization process was also not considered. Basic parameters of the model were set as following: (1) HCl-4-HU, H_2SO_4-4-HU, and H_3PO_4-4-HU were used as simulated object, (2) initial concentrations of HCl-4-HU, H_2SO_4-4-HU, and H_3PO_4-4-HU were same as Table 1, the temperature was 25 °C, and the mass and volume were 1 kg and 1 L, respectively, (3) multiple crystallization reaction equations of Eq. 4–13 were defined and the specific thermodynamic parameter values were referred in Table S1 (Abdel Wahed et al. 2015), (4) two reaction processes of H_2O removal were designed for completely simulating HU evaporation-crystallization process, the first reaction was that 52.725 mol H_2O in 1 L (55.5 mol) HU was removed in 40 steps, the second reaction was that 2.22 mol of H_2O in 2.725 mol HU was removed in 10 steps. In the first 40 steps, CF_V of HU increased from 1 to 20, and then CF_V of HU increased from 20 to 100 in the last 10 steps. Furthermore, reaction temperature of the above two reaction steps was set at 65 °C. (5) The solution was equilibrated with a partial CO_2 pressure of $10^{-3.5}$ atmospheres, and the following mineral phases, such as NaCl, KCl, NH_4Cl, $(NH_4)_2SO_4$, Na_2SO_4, K_2SO_4, and $NH_4H_2PO_4$, were allowed to precipitate out when (and if) they became oversaturated (Abdel Wahed et al. 2014).

$$Na^+ + Cl^- = NaCl \quad (4)$$

$$K^+ + Cl^- = KCl \quad (5)$$

$$NH_4^+ + Cl^- = NH_4Cl \quad (6)$$

$$2NH_4^+ + SO_4^{2-} = (NH_4)_2SO_4 \quad (7)$$

$$NH_4^+ + HSO_4^- = NH_4HSO_4 \quad (8)$$

$$2Na^+ + SO_4^{2-} = Na_2SO_4 \quad (9)$$

$$2Na^+ + SO_4^{2-} + 10H_2O = Na_2SO_4{\cdot}10H_2O \quad (10)$$

$$NH_4^+ + Na^+ + SO_4^{2-} = NH_4NaSO_4 \quad (11)$$

$$NH_4^+ + H_2PO_4^- = NH_4H_2PO_4 \quad (12)$$

$$Na^+ + H_2PO_4^- = NaH_2PO_4 \quad (13)$$

Analytical methods

The concentrations of total ammonia (TAN) and total phosphate (TPO_4^{3-}) in HU were detected by a UV-vis spectrophotometer (UV; Pharo300, Merck, Germany) using the method of Nessler's reagent and ascorbic acid spectrophotometry, respectively (Roé-Sosa et al. 2019). Total carbonate (TCO_3^{2-}) in HU was determined by a TOC analyzer (Multi N/C 2100, Analytik Jena, Germany). The concentration of K^+, Na^+, Cl^-, and SO_4^{2-} were analyzed with ion chromatography (792 Basic IC, Metrohm, Switzerland) (Xie et al. 2017). Electrode and handheld meters were used to measure pH and EC (HQ40d, HACH, USA). Furthermore, the software of PHREEQC-2 was used for simulating the variation of ion concentration in HU during ECP (Abdel Wahed et al. 2014). All tests were performed three times and the data were expressed as the mean of the observed values and followed by the standard deviation (±SD).

Results and discussion

Variation of physico-chemical properties during ECP

pH and EC

Figure 2 shows the variation of pH and EC in HCl-4-HU, H_2SO_4-4-HU, and H_3PO_4-4-HU with the increase in CF_V during ECP. When CF_V increased from 1 to 50, the pH of HCl-4-HU, H_2SO_4-4-HU, and H_3PO_4-4-HU decreased from 4.0 to 1.89, 0.92 and 2.60, and EC increased from 60.40 mS/cm, 56.12 mS/cm, and 74.28 mS/cm to 1054.37 mS/cm, 1165.57 mS/cm, and 1296.87 mS/cm, respectively. Among them, pH in H_3PO_4-4-HU decreased the slowest, and EC in H_3PO_4-4-HU increased the fastest, since H_3PO_4 is a weak electrolyte and H_3PO_4-4-HU has a strong buffer; hence, the required quantity of H_3PO_4 was the maximum (Jiang et al. 2017).

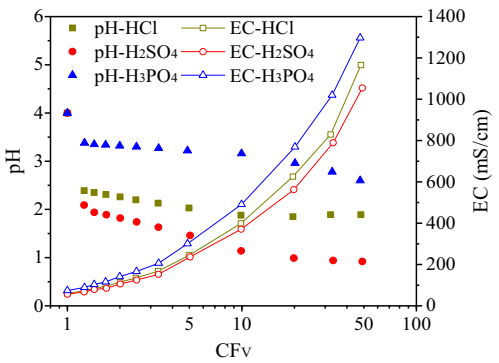

Fig. 2 Variation of pH and EC in HCl-4-HU, H_2SO_4-4-HU, and H_3PO_4-4-HU with increase of CF_V during ECP

Main ion concentration

Figure 3 shows the variation of main ion concentrations in HCl-4-HU, H_2SO_4-4-HU, and H_3PO_4-4-HU with the increase in CF_V during ECP. As shown in Fig. 3a, when $CF_V \leq 4.93$, the concentration of TAN in HCl-4-HU increased and the corresponding $CF_{N\text{-}TAN}$ remained at approximately 1.0. When $4.93 < CF_V \leq 10.04$, the TAN concentration of HCl-4-HU still increased, but the corresponding $CF_{N\text{-}TAN}$ began to decrease. When $CF_V > 10.04$, the TAN concentration and $CF_{N\text{-}TAN}$ presented a downward trend. Based on this phenomenon and the chemical divide rule (Marion 1998), the crystal associated with NH_4^+ should be precipitated before $CF_V = 10.04$. Furthermore, the concentrations of Na^+ and K^+ linearly increased, and the corresponding $CF_{N\text{-}Na}$ and $CF_{N\text{-}K}$ maintained at 1.0 during entire evaporation period, which indicates that no crystal associated with Na^+ and K^+ reached saturation until $CF_V = 48.08$. The general trend of Cl^- concentration was identical to that of TAN, which indicates that the precipitated crystal associated with NH_4^+ should be NH_4Cl at $CF_V = 10.04$. However, $CF_{N\text{-}Cl}$ had no significant downward trend as $CF_{N\text{-}TAN}$ at $CF_V = 10.04$, which indicates that NH_4Cl crystals in HCl-4-HU began to precipitate after $CF_V = 10.04$. In addition, the Cl^- concentration first slightly decreased and subsequently increased, and the TAN concentration continuously decreased while $CF_V > 10.04$, since the Cl^- molar concentration was higher than NH_4^+ in HCl-4-HU, and a large amount of Cl^- was still dissolved in the solution after NH_4Cl completely crystallized. During the entire ECP, the SO_4^{2-} and TPO_4^{3-} concentrations in HCl-4-HU uniformly increased, and their corresponding $CF_{N\text{-}SO4}$ and $CF_{N\text{-}TPO4}$ were maintained at approximately 1.0, which indicates that there was no crystal precipitation associated with SO_4^{2-} and $PO_4^{3-}/HPO_4^{2-}/H_2PO_4^-$ while $CF_V = 48.08$. In conclusion, only NH_4Cl precipitated when HCl-4-HU was concentrated to 48.08 times, and the critical CF_V was 10.04.

As shown in Fig. 3b, when $CF_V \leq 9.90$, the concentrations of TAN and Na^+ in H_2SO_4-4-HU linearly increased, and the corresponding $CF_{N\text{-}TAN}$ and $CF_{N\text{-}Na}$ remained at approximately 1.0. When $CF_V > 19.84$, the TAN and Na^+ concentrations of H_2SO_4-4-HU still increased, but their corresponding CF_N began to decrease in different degrees, which indicates that the crystal associated with NH_4^+ and Na^+ should precipitate after $CF_V = 19.84$ in H_2SO_4-4-HU according to the chemical divide rule (Marion 1998). Furthermore, the K^+ concentration linearly increased, and the corresponding $CF_{N\text{-}K}$ remained at 1.0 during the entire ECP, which indicates that no crystal associated with K^+ reached saturation until $CF_V = 49.02$. The general trend of the Cl^- concentration was identical to those of TAN and Na^+, which indicates that the precipitated crystal associated with NH_4^+ and Na^+ should be NH_4Cl and NaCl at $CF_V \geq 19.84$, due to the chemical divide rule and the smaller Cl^- molar concentration than NH_4^+ and Na^+ in H_2SO_4-4-HU. In addition, the SO_4^{2-} concentration in H_2SO_4-4-HU first decreased, subsequently increased, and finally decreased. The first decrease was due to the strong oxidizing property of H_2SO_4. The SO_4^{2-} concentration increased with the increase in CF_V, the crystal associated with SO_4^{2-} was separated possibly while $CF_V \geq 9.90$, and the precipitated crystals should be $(NH_4)_2SO_4$ or Na_2SO_4. During the entire ECP, the TPO_4^{3-} concentration in H_2SO_4-4-HU was uniformly increasing, and the corresponding $CF_{N\text{-}TPO4}$ remained at approximately 1.0, which indicates that there was no crystal precipitation associated with $PO_4^{3-}/HPO_4^{2-}/H_2PO_4^-$ while $CF_V = 49.02$. Based on the above analysis, $(NH_4)_2SO_4$, Na_2SO_4, NH_4Cl, and NaCl were successively separated at $CF_V = 9.9$ and 19.84 during the entire ECP of H_2SO_4-4-HU.

As was showed in Fig. 3c, when $CF_V \leq 9.90$, the concentration of TAN in H_3PO_4-4-HU was increasing linearly and the corresponding $CF_{N\text{-}TAN}$ maintained at around 1.0, and then the TAN concentration was still increased but the corresponding $CF_{N\text{-}TAN}$ was presented a downward trend, indicating the crystal associated with NH_4^+ should be precipitated out after $CF_V \geq 9.90$ based on the chemical divide rule (Marion 1998). The overall variation trend of Na^+ concentration was similar with TAN but the corresponding $CF_{N\text{-}Na}$ began to decline at $CF_V = 47.62$, indicating the crystal associated with Na^+ separated out later than crystal associated with NH_4^+ in H_3PO_4-4-HU. However, the concentration of K^+ was increasing linearly and the corresponding $CF_{N\text{-}K}$ also maintained at 1.0 during whole evaporation period, indicating that no crystal associated with K^+ precipitated until $CF_V = 47.62$. Besides, the general trend of Cl^- concentration was same with Na^+ and the corresponding $CF_{N\text{-}Cl}$ began to decrease at $CF_V = 47.62$, indicating the precipitated crystal associated with Na^+ should be NaCl around $CF_V = 47.62$. The concentration of SO_4^{2-} in H_3PO_4-4-HU was presented the variation tendency of decline firstly and then increase, the first "decline" was because of reduction reaction of SO_4^{2-} and then the concentration of SO_4^{2-} was upward with the increase of CF_V. In addition, the variation tendency of TPO_4^{3-} concentration and the corresponding $CF_{N\text{-}TPO4}$ were similar with TAN, indicating the crystal associated with NH_4^+ should be $NH_4H_2PO_4$ after $CFV \geq 9.90$ due to that the pH of H_3PO_4-4-HU was less than 4 (Fig. 2) and the main form of phosphate was $H_2PO_4^{3-}$ (Jiang et al. 2016). On the other hand, the molar concentration of TPO_4^{3-} was less than NH_4^+ in H_3PO_4-4-HU, which could further explain the phenomenon of increasing NH_4^+ concentration but declining TPO_4^{3-} concentration after the crystal had been precipitated. From the above, $NH_4H_2PO_4$ and NaCl were successively separated out at $CF_V = 9.9$ and 47.62 during whole ECP of H_3PO_4-4-HU.

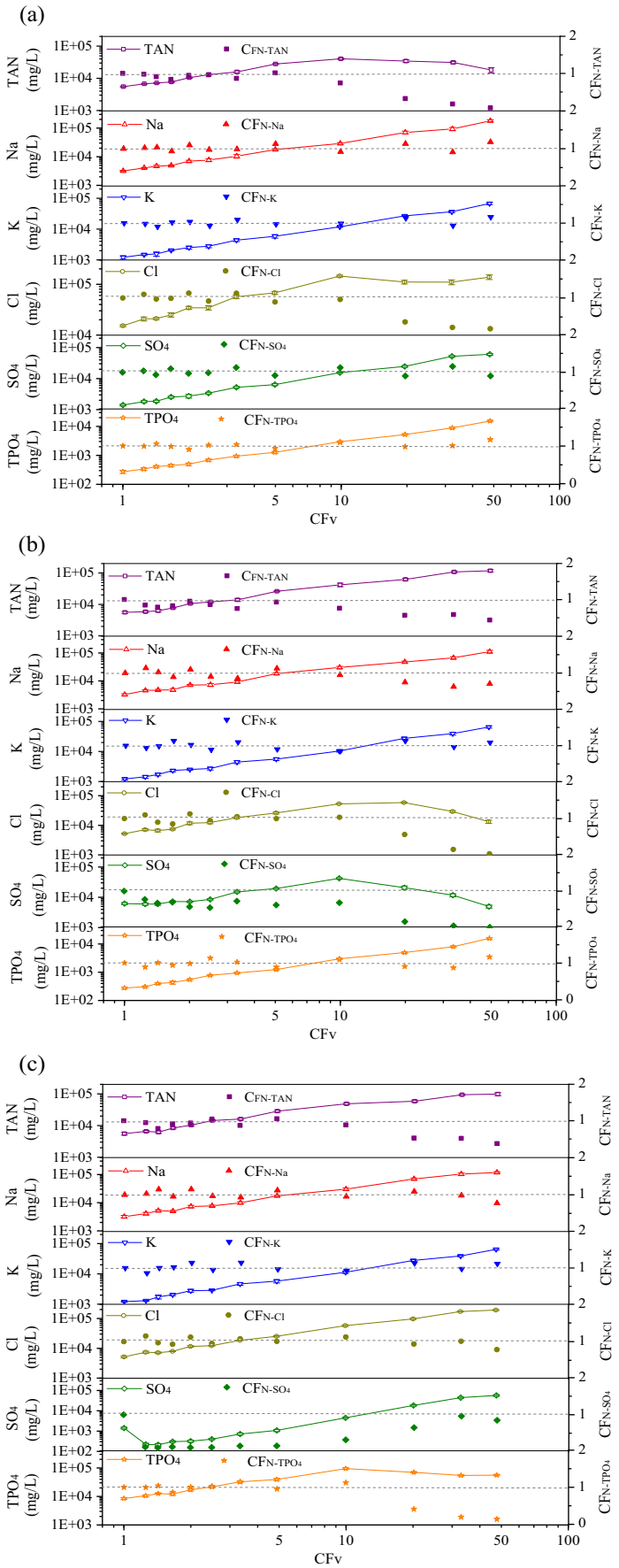

Fig. 3 Variation of main ion concentrations in HCl-4-HU (**a**), H_2SO_4-4-HU (**b**), and H_3PO_4-4-HU (**c**) with increase of CF_V during ECP

Analysis of crystallization thermodynamic properties during ECP

Ion strength (I) and ion activity coefficient (γ) of the main ions such as NH_4^+, Na^+, K^+, Cl^-, SO_4^{2-}, and $H_2PO_4^-$ during ECP of HCl-4-HU, H_2SO_4-4-HU, and H_3PO_4-4-HU were calculated according to *Pitzer model* (Hajbi et al. 2011), and the detail data were shown in supplementary materials (Table S2). The IAP of potential electrolyte crystals during the ECP of HCl-4-HU, H_2SO_4-4-HU, and H_3PO_4-4-HU was further calculated from the data in Table S2, and the relationship between logIAP and CF_V of three HUs is shown in Fig. 4 and Figs. S1-S3. From these curves, the salts that have been crystallized during the ECP can be identified; when the IAP of the considered electrolyte reaches or exceeds the solubility product (Ks), the salt precipitates (Cao et al. 2020; Hajbi et al. 2011).

As was shown in Fig. 4a, logIAP of NaCl almost linearly increased with increasing CF_V, and which was close to the value of logKs (1.5) at CF_V = 48.08, and NaCl crystal should be separated with higher concentration of HCl-4-HU according to the rising trend (Cao et al. 2020). In addition, the corresponding CF_V of HCl-4-HU was 19.61 when logIAP of NH_4Cl reached 0.96 (Ks of NH_4Cl) (Li et al. 2019a), which indicates that NH_4Cl crystal precipitated at CF_V = 19.61 (Fig. 4b). The gap between the maximum of log IAP and logKs was obvious in Fig. S1b, which indicates that no KCl crystal

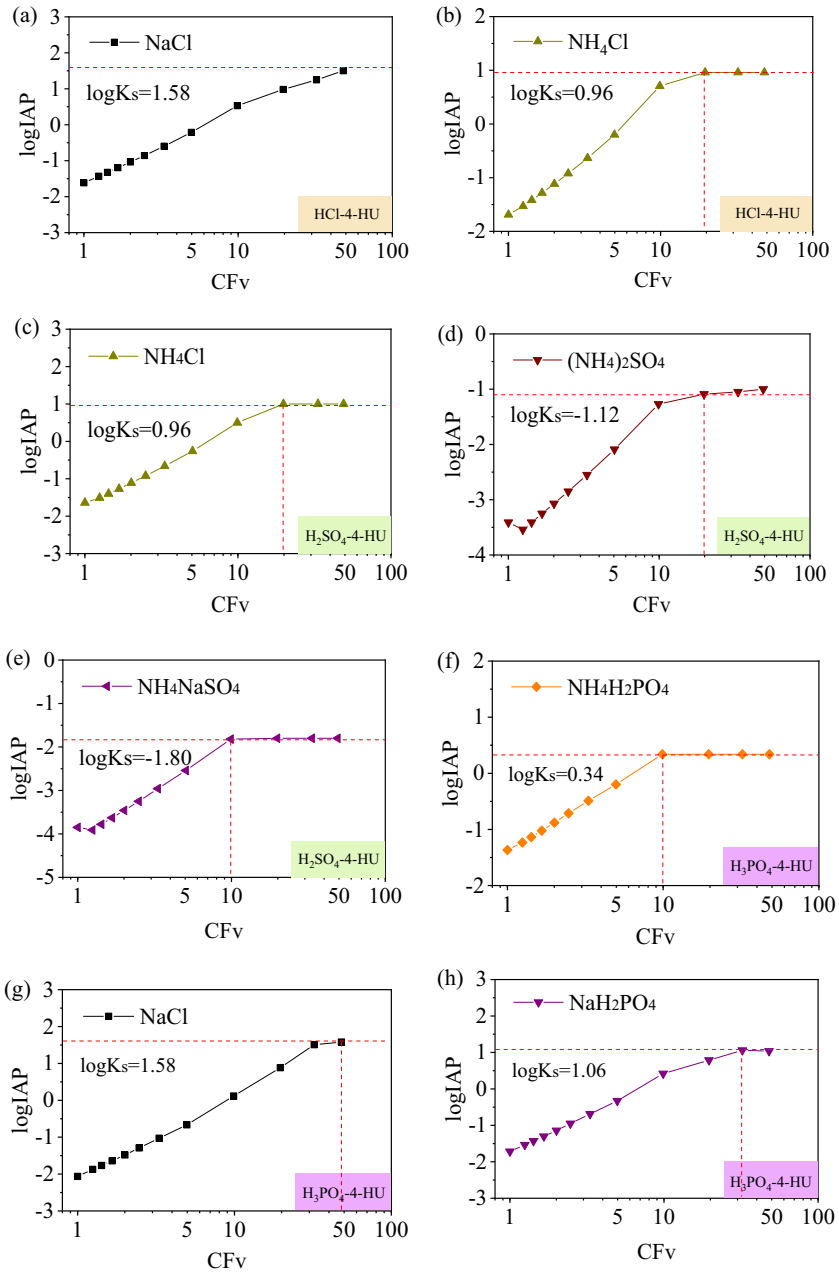

Fig. 4 Relationship between logIAP and CF_V of NaCl (**a**), NH_4Cl (**b**) in HCl-4-HU, NH_4Cl (**c**), $(NH_4)_2SO_4$ (**d**), NH_4NaSO_4 (**e**) in H_2SO_4-4-HU, and $NH_4H_2PO_4$ (**f**), NaCl (**g**), NaH_2PO_4 (**h**) in H_3PO_4-4-HU with increase of CF_V during ECP

separated during the ECP of HCl-4-HU until CF_V = 48.08. The concentrations of NH_4^+ and Cl^- were 34505.87 mg-N/L and 110401.33 mg-Cl/L, respectively, which were significantly less than their maximum saturation concentrations in the "Variation of physico-chemical properties during ECP" section (Fig. 3a). The calculation results relatively lagged behind the experimental data possibly because NH_4Cl crystal was separated at CF_V = 9.88–19.61.

The logIAP of NH_4Cl and $(NH_4)_2SO_4$ gradually increased with the increase in CF_V (Fig. 4c and d), and both CF_V values were 19.84 when their logIAP were 0.96 and − 1.12, which indicates that NH_4Cl and $(NH_4)_2SO_4$ crystals started to precipitate when CF_V of H_2SO_4-4-HU was 19.84. In addition, logIAP and Ks of NH_4NaSO_4 intersected at CF_V = 9.90, which indicates that a portion of NH_4NaSO_4 crystals was acquired before the precipitation of NH_4Cl and $(NH_4)_2SO_4$ crystals in H_2SO_4-4-HU (Fig. 4e). Based on the above analysis, NH_4NaSO_4, $(NH_4)_2SO_4$, and NaCl successively separated at CF_V of 9.90, 19.84, and 19.84, respectively. However, no intersection between logIAP variation curve and Ks occurred during the entire ECP of H_2SO_4-4-HU in Figs. S2 a, d, f, g and h, which implies that NH_4HSO_4, NaCl, $Na_2SO_4{\cdot}10H_2O$, KCl, and Na_2SO_4 were still dissolved, and no related crystals precipitated (Cao et al. 2020; Hajbi et al. 2011). The NH_4^+, Na^+, and SO_4^{2-} concentrations in NH_4NaSO_4 crystals were 42098.97 mg-N/L, 30176.82 mg-Na/L, and 42070.02 mg/L, and the NH_4^+, SO_4^{2-}, Na^+, and Cl^- concentrations in $(NH_4)_2SO_4$ and NaCl crystals were 62575.30 mg-N/L, 20841.46 mg/L, 47667.04 mg-Na/L, and 58845.59 mg/L, respectively (Fig. 3b).

CF_V of H_3PO_4-4-HU was 9.96 when logIAP of $NH_4H_2PO_4$ reached its logKs value (0.34), which indicates that $NH_4H_2PO_4$ crystal should separate in H_3PO_4-4-HU (Fig. 4f). The relationship between logIAP of NaCl and NaH_2PO_4 and their logKs is shown in Fig. 4g and h, respectively. The corresponding CF_V values of the internode were 47.62 and 32.89, which indicates that NaH_2PO_4 and NaCl crystals successively precipitated after $NH_4H_2PO_4$ was obtained. Furthermore, logIAP of NH_4Cl was close to but logIAP of KCl was far away from their logKs values at CF_V = 47.62. According to the rising trend of logIAP, we can speculate that NH_4Cl crystal should be dissolved, and no KCl was obtained at higher CF_V (Fig. S3 a and d). In conclusion, $NH_4H_2PO_4$, NaH_2PO_4, and NaCl successively separated at CF_V of 9.96, 32.89, and 47.62, respectively. The maximum saturation concentrations of NH_4^+ and $H_2PO_4^-$ were 48874.66 mg-N/L, and 95028.02 mg-P/L when $NH_4H_2PO_4$ was separated. The maximum saturation concentrations of Na^+ and $H_2PO_4^-$ were 103395.58 mg-Na/L and 54606.89 mg-P/L when NaH_2PO_4 was separated. The maximum saturation concentrations of Na^+ and Cl^- were 117953.48 mg-Na/L and 192863.73 mg/L, respectively (Fig. 3c).

Analysis of crystallization sequence

The crystal components are complicated due to the variety of inorganic salts in HU, and it was difficult to accurately obtain the crystallization period and precipitated mass of each electrolyte. On the other hand, the experimental error caused by the sampling is not also conducive to the crystallization of the real crystallization process of HU. Thus, PHREEQC-2 was used to chemically simulate the ECP of HCl-4-HU, H_2SO_4-4-HU, and H_3PO_4-4-HU, and the crystallization sequence and mass of each crystal were inferred from this analysis.

The simulated value and measured value of TAN, Na^+, K^+, Cl^-, and SO_4^{2-} and TPO_4^{3-} concentration during the ECP of

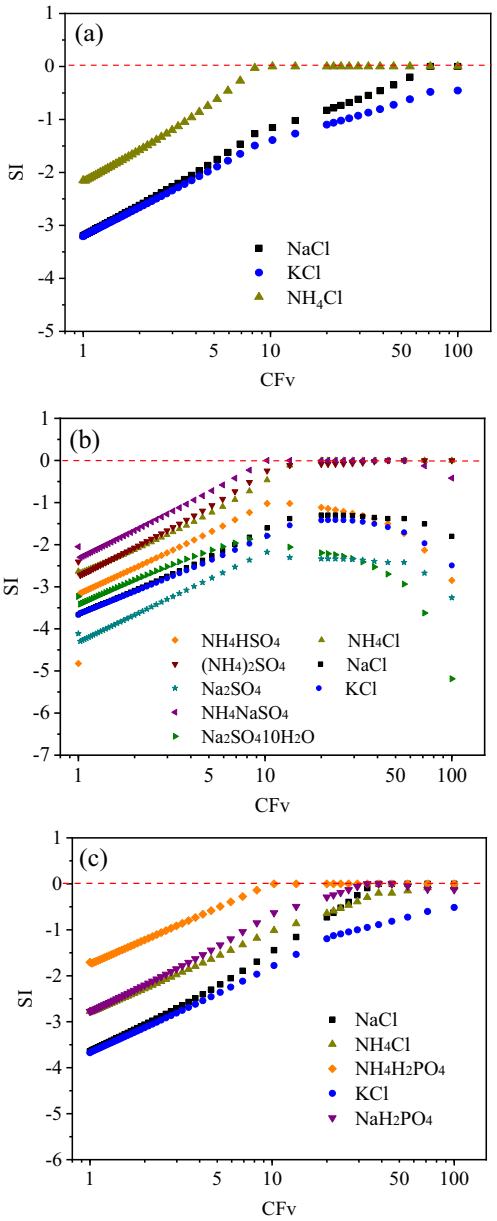

Fig. 5 Evolution of mineral saturation indices (SI) during ECP of **a** HCl-4-HU, **b** H_2SO_4-4HU, and **c** H_3PO_4-4-HUsimulated by PHREEQC-2

Table 3 The crystalline type and content of precipitated crystal during each concentration stage of HCl-4-HU, H_2SO_4-4-HU, and H_3PO_4-4-HU

	CF_V range	Crystalline type	Content	
			Mass concentration (mg/L)	Percentage (%)
HCl-4-HU	10.25~100	NH_4Cl	63.60	98
	71.43~100	NaCl	1.39	2
H_2SO_4-4-HU	10.25~55.56	NH_4NaSO_4	17.16	30
	20~100	NH_4Cl	32.12	56
	45.46~100	$(NH_4)_2SO_4$	7.66	14
H_3PO_4-4-HU	10.25~100	$NH_4H_2PO_4$	94.53	81
	38.46~55.56	NaH_2PO·	1.80	6
	45.45~100	NaCl	15.25	13

HCl-4-HU, H_2SO_4-4-HU, and H_3PO_4-4-HU were compared in supplementary materials (Fig. S4, S5 and S6), respectively. It was obvious that the measured value was mainly in the range of 95~105% of the simulated value for each ion concentration at different CF_V of three HU, indicating that the calculation results based on the initial conditions of section 2.4 by PHRREEQC-2 were credible, and it could precisely express the ion concentration and crystallization situation of mineral salts when CF_V increased to 100 in HU.

Figure 5a~c showed the evolution of mineral saturation indices (SI) during ECP of HCl-4-HU, H_2SO_4-4HU, and H_3PO_4-4-HU, which were simulated by PHREEQC-2. The crystalline type and molar mass of precipitated crystal in each concentration stage of HCl-4-HU, H_2SO_4-4-HU, and H_3PO_4-4-HU are listed in Table 3. SI of NH_4Cl and NaCl crystals successively reached 0 at CF_V of 10.25 and 71.43, respectively, but SI of KCl was less than 0, which indicates that the NH_4Cl and NaCl crystals should separate at CF_V of 10.25 and 71.43 in HCl-4-HU (Fig. 5a) (Abdel Wahed et al. 2014). The masses of NH_4Cl and NaCl crystals obtained at CF_V of 10.25~100 and 71.43~100 were 63.60 g/L and 1.39 g/L, respectively (Table 3). Similar results are obtained from Fig. 5b and c. The NH_4NaSO_4, NH_4Cl, and $(NH_4)_2SO_4$ crystals should be separated at CF_V of 10.25, 20.00, and 40.45 in H_2SO_4-4-HU, and the masses of NH_4NaSO_4, NH_4Cl, and $(NH_4)_2SO_4$ crystals obtained at CF_V of 10.25~55.56, 20~100, and 45.46~100 were 17.16 g/L, 32.12 g/L, and 7.66 g/L, respectively (Table 3). Similarly, the $NH_4H_2PO_4$, NaH_2PO_4, and NaCl crystals should separate at CF_V of 10.25, 38.46, and 45.45 in H_2SO_4-4-HU (Fig. 5c). The masses of $NH_4H_2PO_4$, NaH_2PO_4, and NaCl crystal obtained at CF_V of 10.25~100, 38.46~55.56, and 45.46~100 were 4.53 g/L, 94.53 g/L, and 15.25 g/L, respectively (Table 3). In a word, crystallization sequence of HCl-4-HU, H_2SO_4-4-HU, H_3PO_4-4-HU during ECP were NH_4Cl (CF_V from 10.25 to 100) / NaCl (CF_V from 71.43 to 100), NH_4NaSO_4 (CF_V from 10.25 to 55.56) / NH_4Cl (CF_V from 20 to 100) / $(NH_4)_2SO_4$ (CF_V from 40.45 to 100), $NH_4H_2PO_4$ (CF_V from 10.25 to 100) / NaH_2PO_4 (CF_V from38.46 to 55.5) / NaCl (CF_V from 45.46 to 100), respectively (Fig. 6), and the main composition and content was consistent with the result of our precious research (Jiang et al. 2017). It was clearly seen that both crystalline product of HCl-4-HU and H_2SO_4-4-HU contain NH_4Cl, but the NH_4Cl precipitation in HCl-4-HU was earlier than in H_2SO_4-4-HU, the main reason was that the higher concentration of Cl^- in HCl-4-HU and Cl^- was the limiting factor for NH_4Cl saturation in HCl-4-HU and H_2SO_4-4-HU. On the other hand, both crystalline products of HCl-4-HU and H_3PO_4-4-HU contain NaCl, but the NaCl precipitation in HCl-4-HU was later than in H_3PO_4-4-HU, which attribute to that NH_4Cl precipitation in HCl-4-HU consumed a lot of Cl^-. In order to improve the practicability of urine crystal products as agricultural fertilizer, NaCl formation should be avoided during the ECP of HU. Therefore, H_2SO_4 was the most recommended pH-adjusted acid for no NaCl formation in crystal products of H_2SO_4-4-HU, and H_3PO_4 was not recommended for high content of NaCl in crystal products. If HCl was chosen as pH-adjusted acid, the CFv of HCl-4-HU should be controlled less than 70.

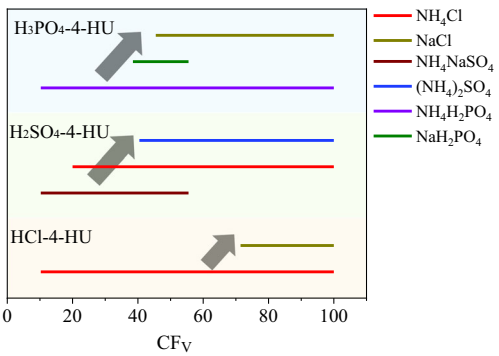

Fig. 6 Comparison of crystallization sequence of HCl-4-HU, H_2SO_4-4-HU, and H_3PO_4-4-HU during ECP

Conclusion

In this study, the effect of pH-adjusted acid on the evaporation and crystallization process of HU was examined. HCl-4-HU, H_2SO_4-4-HU, and H_3PO_4-4-HU had significantly different crystallization thermodynamic characteristics, crystallization sequence, and crystallization products. The first appearance of the new crystal in HCl-4-HU, H_2SO_4-4-HU, and H_3PO_4-4-HU occurred CF_V of 19.61, 9.90, and 9.96, respectively. Furthermore, the simulated crystallization process characteristics of HU by PHREEQC-2 have a good fit with the actual experimental data, and crystallization sequence of HCl-4-HU, H_2SO_4-4-HU, H_3PO_4-4-HU during ECP were NH_4Cl (CF_V from 10.25 to 100) / NaCl (CF_V from 71.43 to 100), NH_4NaSO_4 (CF_V from 10.25 to 55.56) / NH_4Cl (CF_V from 20 to 100) / $(NH_4)_2SO_4$ (CF_V from 40.45 to 100), $NH_4H_2PO_4$ (CF_V from 10.25 to 100) / NaH_2PO_4 (CF_V from38.46 to 55.5) / NaCl (CF_V from 45.46 to 100), respectively. In order to avoid NaCl formation during the ECP of HU, H_2SO_4 was the most recommended pH-adjusted acid for acidification of HU. If HCl was chosen as pH-adjusted acid, the CFv of HCl-4-HU should be controlled less than 70. In a word, the present study provides an important theoretical basis for the optimization of crystallized products obtained from HU in the future.

Supplementary Information The online version of this article (https://doi.org/10.1007/s11356-021-12598-2) contains supplementary material, which is available to authorized users.

Author contributions Shanqing Jiang: conceptualization, investigation, methodology, formal analysis, writing – original draft, writing – review and editing, project administration, funding acquisition
Xiang Xing: data curation, software, funding acquisition
Liping Wang: resources
Shengjiong Yang: software
Jingwen Xiao: data curation
Qiuya Zhang: software
Xia Xu: software
Mingguo Peng: resources
Xiaochang Wang: supervision, project administration

Funding This work was supported by the Major Basic Research Project of the Natural Science Foundation of the Jiangsu Higher Education Institutions (19KJB560008), Changzhou Sci&Tech Program (CJ20200077), and Postgraduate Research & Practice Innovation Program of Jiangsu Province (KYCX20_2601).

Data availability All data generated or analyzed during this study are included in this published article [and its supplementary information files].

Declarations

Ethics approval and consent to participate Not applicable.

Consent for publication Written informed consent for publication was obtained from all participants.

Conflict of interest The authors declare no competing interests.

References

Abdel Wahed MSM, Mohamed EA, El-Sayed MI, M'Nif A, Sillanpää M (2014) Geochemical modeling of evaporation process in Lake Qarun, Egypt. J Afr Earth Sci 97:322–330. https://doi.org/10.1016/j.jafrearsci.2014.05.008

Abdel Wahed MSM, Mohamed EA, El-Sayed MI, M'Nif A, Sillanpää M (2015) Crystallization sequence during evaporation of a high concentrated brine involving the system Na–K–Mg–Cl–SO_4-H_2O. Desalination 355:11–21. https://doi.org/10.1016/j.desal.2014.10.015

Alemayehu YA, Asfaw SL, Terfie TA (2020) Nutrient recovery options from human urine: a choice for large scale application. Sustainable Production and Consumption 24:219–231. https://doi.org/10.1016/j.spc.2020.06.016

Antonini S, Nguyen PT, Arnold U, Eichert T, Clemens J (2012) Solar thermal evaporation of human urine for nitrogen and phosphorus recovery in Vietnam. Sci Total Environ 414:592–599. https://doi.org/10.1016/j.scitotenv.2011.11.055

Barbosa SG, Peixoto L, Meulman B, Alves MM, Pereira MA (2016) A design of experiments to assess phosphorous removal and crystal properties in struvite precipitation of source separated urine using different Mg sources. Chem Eng J 298:146–153. https://doi.org/10.1016/j.cej.2016.03.148

Cao J, Ren Y, Yu B, Zhu Q, Zhang Y (2020) Solid-liquid phase equilibria of quaternary systems $Na^+//Cl^-$, CO_3^{2-}, SO_4^{2-} - H_2O and $Na^+//Cl^-$, CO_3^{2-}, NO_3^- - H_2O at T = 313.15 K. J Chem Thermodyn 142:106028. https://doi.org/10.1016/j.jct.2019.106028

Chipako TL, Randall DG (2020) Investigating the feasibility and logistics of a decentralized urine treatment and resource recovery system. J Water Process Eng 37:101383. https://doi.org/10.1016/j.jwpe.2020.101383

Gulyas H, Bruhn P, Furmanska M, Hartrampf K, Kot K, Luttenberg B, Mahmood Z, Stelmaszewska K, Otterpohl R (2004) Freeze concentration for enrichment of nutrients in yellow water from no-mix toilets. Water Sci Technol 50:61–68. https://doi.org/10.2166/wst.2004.0360

Hajbi F, Hammi H, Solimando R, M'nif A (2011) Evaporation of a reverse osmosis discharge studied by Pitzer model and solubility phase diagrams. Fluid Phase Equilib 307:126–134. https://doi.org/10.1016/j.fluid.2011.04.014

Huang H, Li J, Li B, Zhang D, Zhao N, Tang S (2019a) Comparison of different K-struvite crystallization processes for simultaneous potassium and phosphate recovery from source-separated urine. Sci Total Environ 651:787–795. https://doi.org/10.1016/j.scitotenv.2018.09.232

Huang H, Zhang D, Wang W, Li B, Zhao N, Li J, Dai J (2019b) Alleviating Na^+ effect on phosphate and potassium recovery from synthetic urine by K-struvite crystallization using different magnesium sources. Sci Total Environ 655:211–219. https://doi.org/10.1016/j.scitotenv.2018.11.259

Jiang S, Wang X, Yang S, Shi H (2016) Characteristics of simultaneous ammonium and phosphate adsorption from hydrolysis urine onto natural loess. Environ Sci Pollut Res 23:2628–2639. https://doi.org/10.1007/s11356-015-5443-1

Jiang SQ, Wang XC, Yang SJ, Shi HL (2017) Effect of initial pH and pH-adjusted acid on nutrient recovery from hydrolysis urine by combining acidification with evaporation-crystallization Environmental Science and Pollution Research 24:3872-3881. https://doi.org/10.1007/s11356-016-8052-8

Karak T, Bhattacharyya P (2011) Human urine as a source of alternative natural fertilizer in agriculture: a flight of fancy or an achievable

reality Resources. Conservation and Recycling 55:400–408. https://doi.org/10.1016/j.resconrec.2010.12.008

Lassin A, André L, Lach A, Thadée A-L, Cézac P, Serin J-P (2018) Solution properties and salt-solution equilibria in the H-Li-Na-K-Ca-Mg-Cl-H2O system at 25 °C: a new thermodynamic model based on Pitzer's equations Calphad 61:126-139. https://doi.org/10.1016/j.calphad.2018.03.005

Ledezma P, Kuntke P, Buisman CJN, Keller J, Freguia S (2015) Source-separated urine opens golden opportunities for microbial electrochemical technologies. Trends Biotechnol 33:214–220. https://doi.org/10.1016/j.tibtech.2015.01.007

Li C, Zhao B, Wang S, Xue C-Y, Guo H-F, Wang D-Y, Cao J-L (2019a) Phase diagrams of the quinary system K^+, NH_4^+, Mg^{2+}// SO_4^{2-}, Cl^--H_2O at 273.15 K and 298.15 K and their application. Fluid Phase Equilib 499:112238. https://doi.org/10.1016/j.fluid.2019.07.001

Li D, Meng L, Guo Y, Deng T, Yang L (2019b) Chemical engineering process simulation of brines using phase diagram and Pitzer model of the system $CaCl_2SrCl_2H_2O$. Fluid Phase Equilib 484:232–238. https://doi.org/10.1016/j.fluid.2018.11.034

Liu J, Zheng M, Wang C, Liang C, Shen Z, Xu K (2020) A green method for the simultaneous recovery of phosphate and potassium from hydrolyzed urine as value-added fertilizer using wood waste Resources. Conservation and Recycling 157:104793. https://doi.org/10.1016/j.resconrec.2020.104793

Malila R, Lehtoranta S, Viskari EL (2019) The role of source separation in nutrient recovery – comparison of alternative wastewater treatment systems. J Clean Prod 219:350–358. https://doi.org/10.1016/j.jclepro.2019.02.024

Marion GM (1998) The geochemistry of natural waters : surface and groundwater environments. Third Edition Journal of Environmental Quality 27:245–246. https://doi.org/10.2134/jeq.1998.00472425002700010037x

Pronk W, Koné D (2009) Options for urine treatment in developing countries. Desalination 248:360–368. https://doi.org/10.1016/j.desal.2008.05.076

Randall DG, Nathoo J (2018) Resource recovery by freezing: a thermodynamic comparison between a reverse osmosis brine, seawater and stored urine. Journal of Water Process Engineering 26:242–249. https://doi.org/10.1016/j.jwpe.2018.10.020

Roé-Sosa A, Rangel-Peraza JG, Rodríguez-Mata AE, Pat-Espadas A, Bustos-Terrones Y, Diaz-Peña I, Vu CM, Amabilis-Sosa LE (2019) Emulating natural wetlands oxygen conditions for the removal of N and P in agricultural wastewaters. J Environ Manag 236:351–357. https://doi.org/10.1016/j.jenvman.2019.01.114

Simha P, Lalander C, Nordin A, Vinnerås B (2020) Alkaline dehydration of source-separated fresh human urine: preliminary insights into using different dehydration temperature and media. Sci Total Environ 733:139313. https://doi.org/10.1016/j.scitotenv.2020.139313

Tao W, Bayrakdar A, Wang Y, Agyeman F (2019) Three-stage treatment for nitrogen and phosphorus recovery from human urine: hydrolysis, precipitation and vacuum stripping. J Environ Manag 249:109435. https://doi.org/10.1016/j.jenvman.2019.109435

Udert KM, Wächter M (2012) Complete nutrient recovery from source-separated urine by nitrification and distillation. Water Res 46:453–464. https://doi.org/10.1016/j.watres.2011.11.020

Volpin F, Yu H, Cho J, Lee C, Phuntsho S, Ghaffour N, Vrouwenvelder JS, Shon HK (2019) Human urine as a forward osmosis draw solution for the application of microalgae dewatering. J Hazard Mater 378:120724. https://doi.org/10.1016/j.jhazmat.2019.06.001

Volpin F, Jiang J, el Saliby I, Preire M, Lim S, Hasan Johir MA, Cho J, Han DS, Phuntsho S, Shon HK (2020) Sanitation and dewatering of human urine via membrane bioreactor and membrane distillation and its reuse for fertigation. J Clean Prod 270:122390. https://doi.org/10.1016/j.jclepro.2020.122390

Wang J, Wei Y (2020) Recovery of monovalent mineral salts from urine in controlled ecological life support system by nanofiltration: feasibility study. Desalination 479:114344. https://doi.org/10.1016/j.desal.2020.114344

Xie J, Liu X, Pan W, Cai C, Ren Y (2017) Phase equilibria in the system Na^+, K^+//SO_4^{2-}-$(CH_2OH)_2$-H_2O and Na^+, K^+//Cl^-, SO_4^{2-}-$(CH_2OH)_2$-H_2O at 328.15K. J Chem Thermodyn 112:155–165. https://doi.org/10.1016/j.jct.2017.05.002

Xu K, Lin F, Dou X, Zheng M, Tan W, Wang C (2018) Recovery of ammonium and phosphate from urine as value-added fertilizer using wood waste biochar loaded with magnesium oxides. J Clean Prod 187:205–214. https://doi.org/10.1016/j.jclepro.2018.03.206

Yang L, Li D, Zhang T, Meng L, Deng T, Guo Y (2020) Thermodynamic phase equilibria in the aqueous ternary system NaCl–$NaBO_2$–H_2O: Experimental data and solubility calculation using the Pitzer model. J Chem Thermodyn 142:106021. https://doi.org/10.1016/j.jct.2019.106021

Zhang Y, Hu B, Teng Y, Tu K, Zhu C (2019) A library of BASIC scripts of reaction rates for geochemical modeling using phreeqc. Comput Geosci 133:104316. https://doi.org/10.1016/j.cageo.2019.104316

Publisher's note Springer Nature remains neutral with regard to jurisdictional claims in published maps and institutional affiliations.